Electronic Supplementary Material (ESI) for Energy & Environmental Science.

Electronic Supplementary Information

Crosslinked Fluoropolymers Exhibiting Superior High-Temperature Energy Density and Charge–Discharge Efficiency

He Li, Matthew R. Gadinski, Yuqi Huang, Lulu Ren, Yao Zhou, Ding Ai, Zhubing Han, Bin Yao and Qing Wang

Department of Materials Science and Engineering, The Pennsylvania State University, University Park, Pennsylvania, 16802, USA.

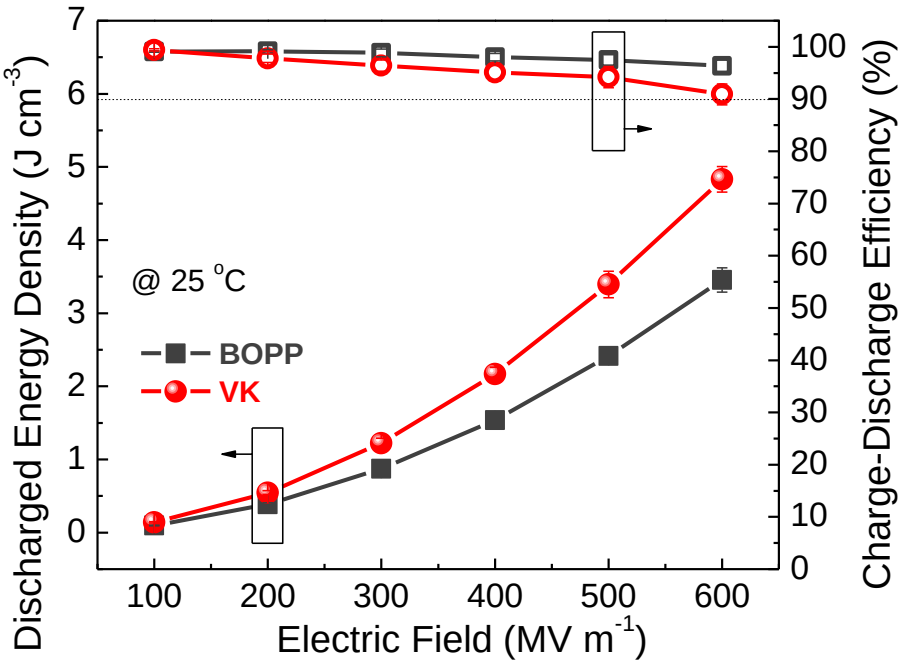

Fig. S1. Discharged energy density and charge–discharge efficiency of BOPP and **VK** at room temperature. Error bars represent standard deviations obtained from at least three measurements using different samples.

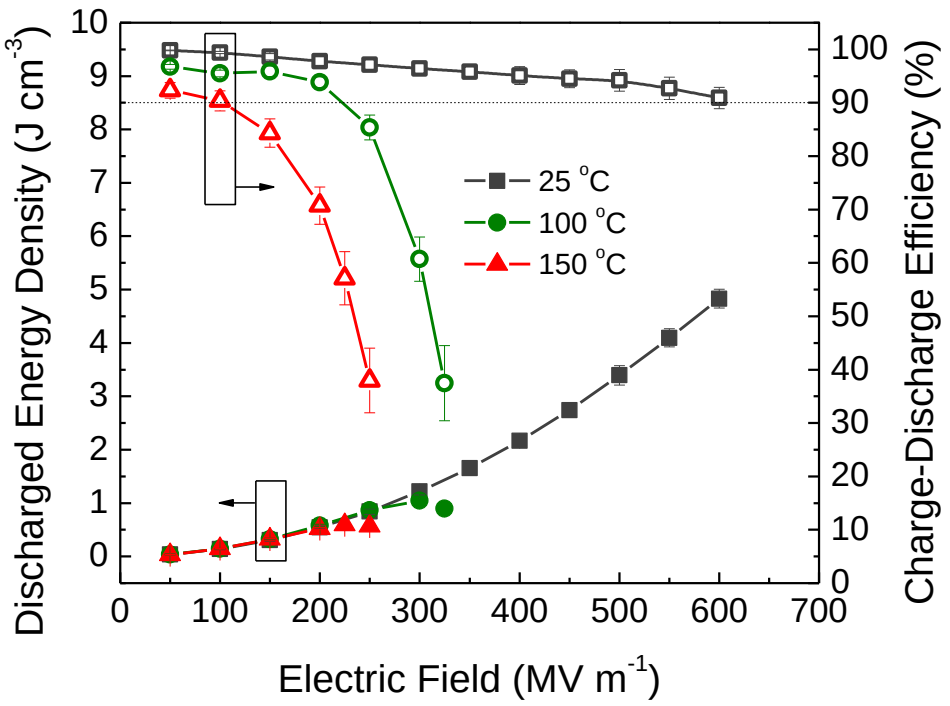

Fig. S2. Discharged energy density and charge–discharge efficiency of **VK** at varied temperatures. Error bars represent standard deviations obtained from at least three measurements using different samples.

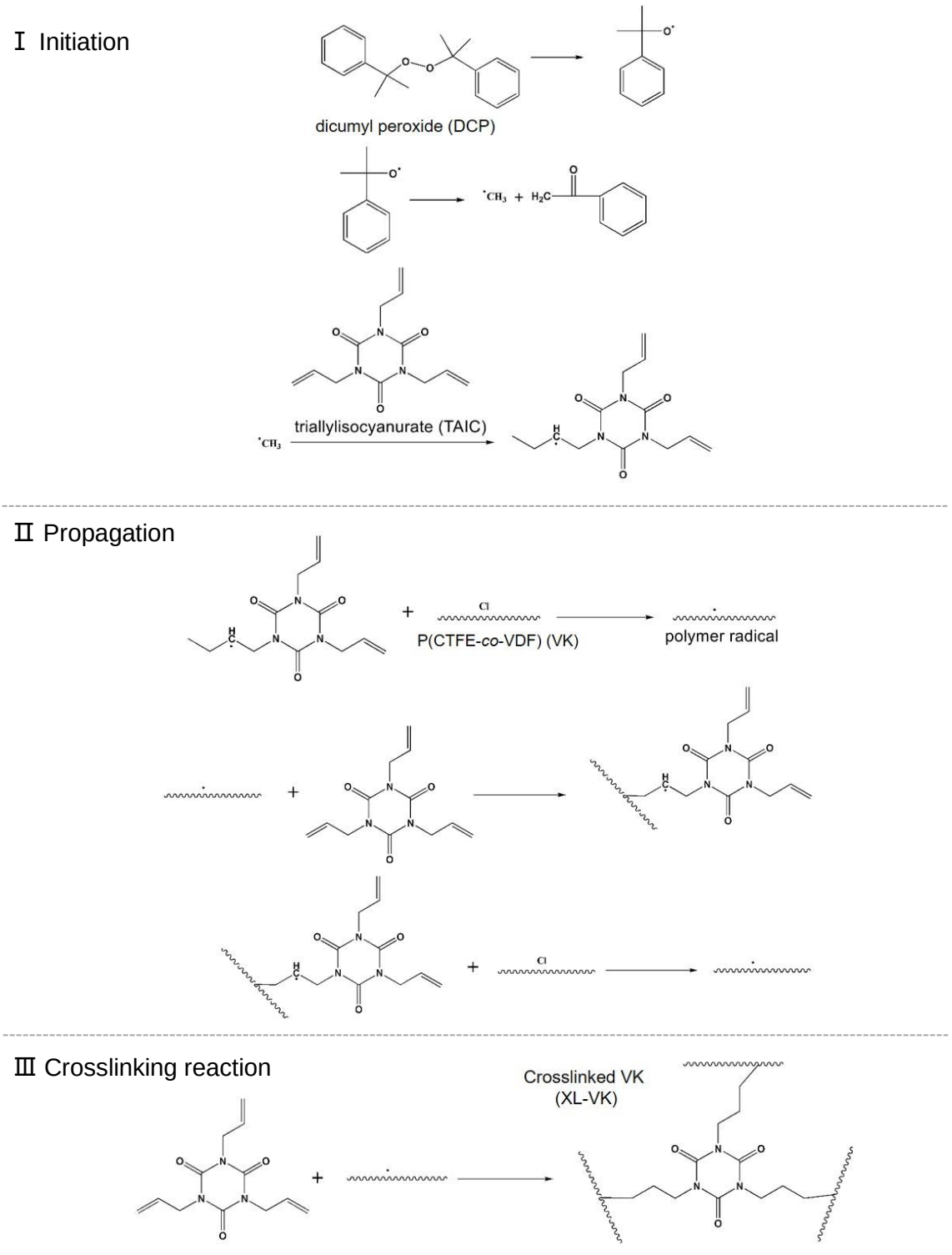

Fig. S3. The mechanism of crosslinking reaction of **XL-VK**.

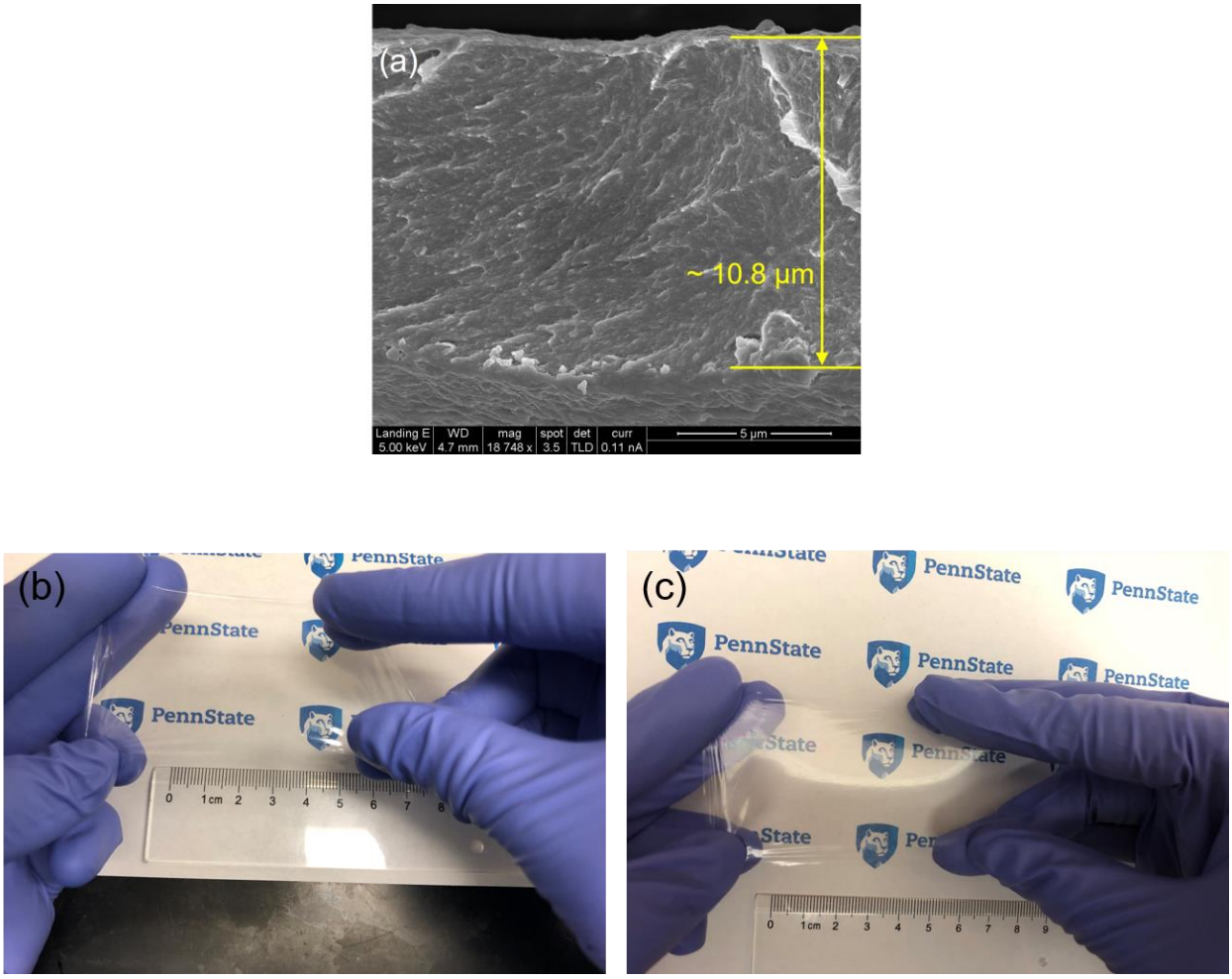

Fig. S4. (a) Cross-sectional SEM image of **XL-VK-2** film with a thickness of 10.8 µm. Photographs of **XL-VL-2** films (b) before and after (c) socking in a high-temperature insulation fluid at 150 ^{o}C for 24 h. The crosslinked films maintain the flatness, transparency and flexibility, exhibiting excellent thermal stability.

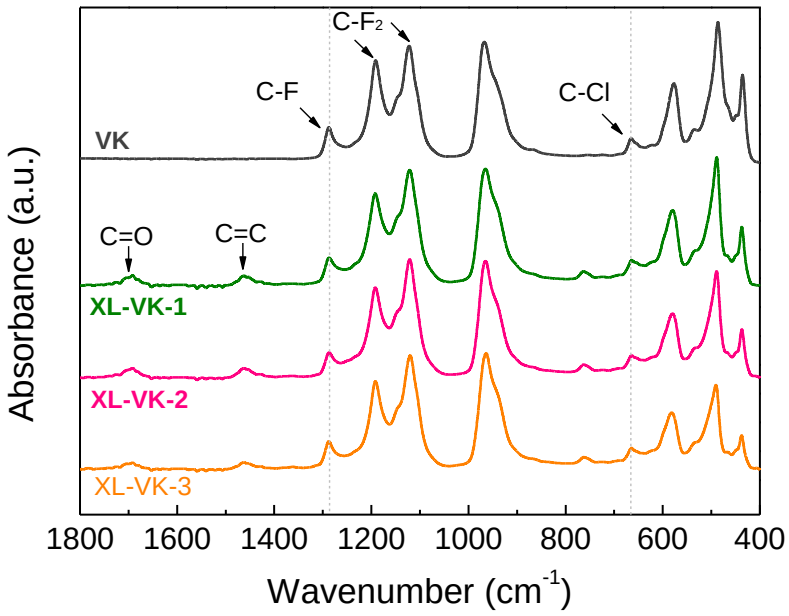

Fig. S5. ATR-FTIR spectra of **VK** and **XL-VK**. The peaks at 1470 cm^{-1} and 1700 cm^{-1} in the XL-VK spectra correspond to the double bond formation and the carbonyl of the triallyl isocyanurate (TAIC), respectively.[1,2] These groups have been shown to act as charge traps in the crosslinked polymers.[3,4] The peaks at 1282 cm^{-1} and 665 cm^{-1} are attributed to the C-F and C-Cl bonds of the polymer backbones, respectively.[2,5,6] The ratio of the intensities of the C-F peak to the C-Cl peak were taken and normalized to 3.05 (to account for the 2.5 mol% VDF in **VK**) for the pristine **VK**.[2] The ratio after crosslinking is 3.13, 3.22 and 3.30 for **XL-VK-1**, **-2**, **-3**, which correspond to a 2.4%, 5.7% and 8.2% decrease in chlorine, respectively.

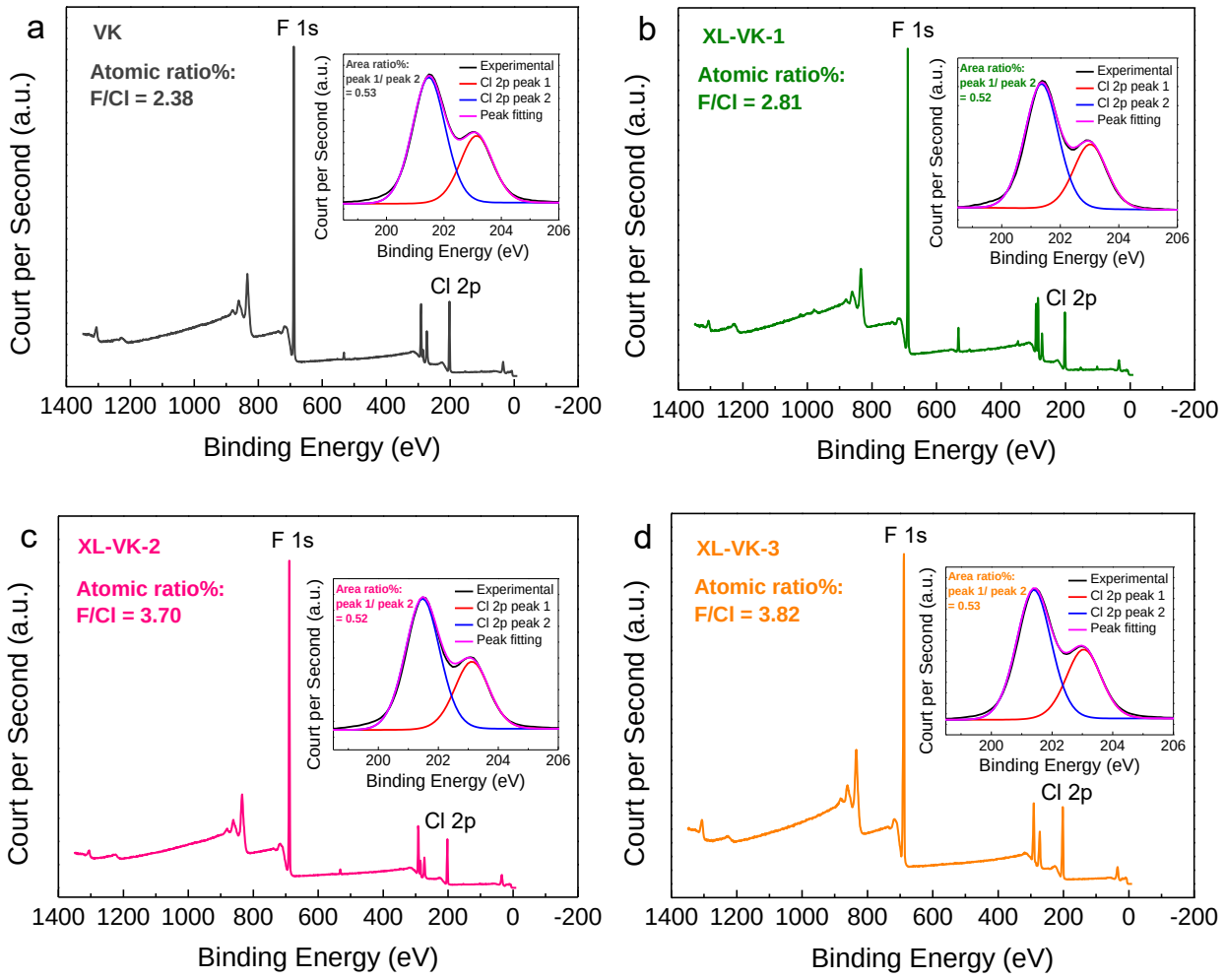

Fig. S6. XPS spectra of **VK** and **XL-VK**. Insets show the high-resolution XPS of Cl 2p. The peaks of Cl 2p were fitted by using "Peak Add" of Thermo Advantage, the area ratios of peak 1/peak 2 are around 0.52~0.53 for all the **VK** and **XL-VK** samples, which indicates that the crosslinking reaction does not change the chemical status of chlorine. The atomic ratio of F/Cl was calculated by using Survey Spectrum of Thermo Advantage, which increases from 2.38 of pristine **VK** to 2.81, 3.70 and 3.82 of **XL-VK-1**, **XL-VK-2**, and **XL-VK-3**, respectively. The increased atomic ratio F/Cl is due the elimination of chlorine groups from chlorotrifluoroethylene because of crosslinking reaction, which is consistent with the trend shown in ATR-FTIR measurements.

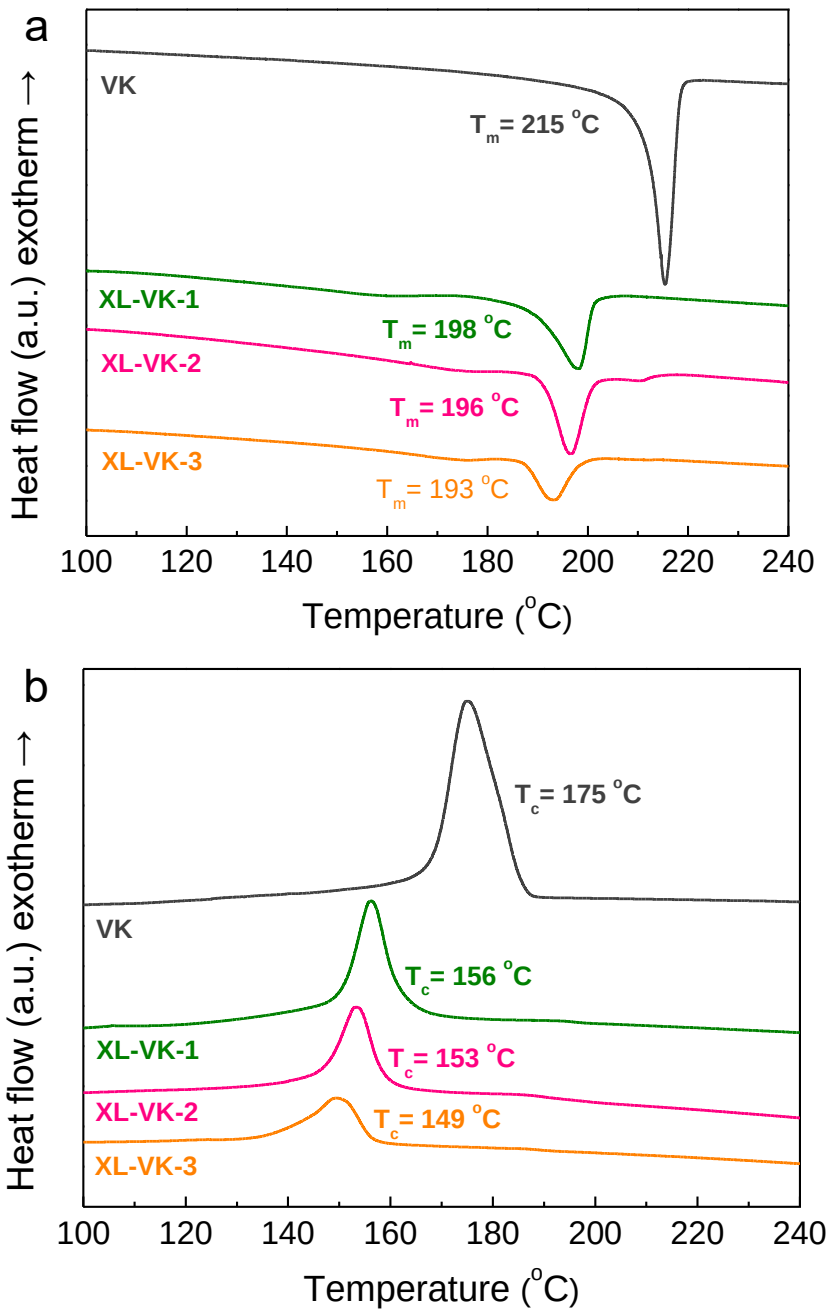

Fig. S7. DSC curves collected during (a) the heating cycle and (b) the cooling cycle of **VK** and **XL-VK**. Crosslinking was found to decrease the melting temperature, the crystallization temperature as well as crystallinity of **XL-VK** with respect to the pristine **VK**. The crystallinity was calculated as[7,8]

$$X_{\mathrm{DSC}} = \frac{\Delta H_s}{\Delta H_0} \times 100\% \qquad \text{(S1)}$$

where X_{DSC} is the calculated crystallinity from DSC curve, ΔH_s is the heat of fusion integrated from melting peak of DSC curve and ΔH_0 of 43 J g^{-1} is the corrected heat of fusion of a 100% crystalline PCTFE.[7,8] This calculation assumes that the heat of fusion is independent of the co-monomer content used here (2.5 mol%). The X_{DSC} was found to drop from 40.1% in pristine **VK** to 21.1%, 19.3% and 10.8% in **XL-VK-1**, **-2** and **-3**. The melting temperature decreases from 215 ^{o}C for pristine **VK** to 198 ^{o}C, 196 ^{o}C and 193 ^{o}C for **XL-VK-1**, **-2** and **-3**. The crystallization temperature decreases from 175 ^{o}C for pristine **VK** to 156 ^{o}C, 153 ^{o}C and 149 ^{o}C for **XL-VK-1**, **-2** and **-3**. Further decrease in melting temperature is relevant as it suggests a decrease in crystallite size[9].

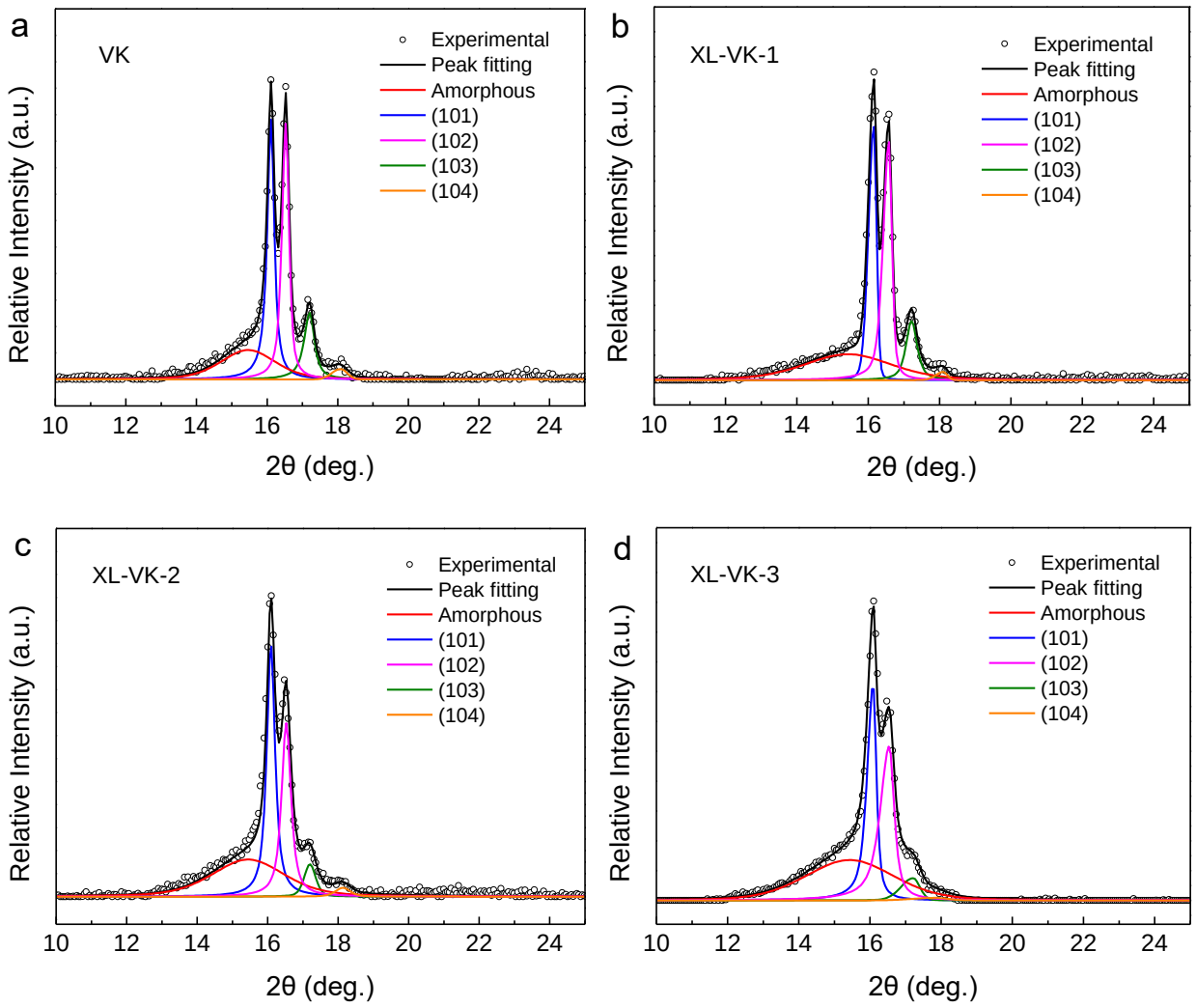

Fig. S8. XRD spectra of **VK** and **XL-VK.** All data were analyzed using Jade software with a Gaussian-Lorentz superposition fitting function. The crystallinity calculated from XRD (X_{XRD}) are consistently higher than that of DSC results.[8] The decrease in crystallite size is also confirmed by the XRD curves, indicating little difference between the pristine and crosslinked polymers, but all show the same crystalline phase of PCTFE. The crystallite size of **XL-VK**, however, is observed to be smaller which is visible in spectra as the broadening of the peaks no longer allows the shoulder of each plane from being visible as they are in pristine **VK**. The spectra of all samples is a result of 4 peaks located at about 16.3°, 16.7°, 17.3°, and 18.2° 2θ corresponding to the (101), (102), (103), and (104) planes, respectively.[8]

Table S1. Crystallographic parameters of **VK** and **XL-VK**.

Sample	Crystallinity by DSC (X_{DSC})	Crystallinity by XRD (X_{XRD})	Crystallite size d(101) (nm)	Crystallite size d(102) (nm)	Crystallite size d(103) (nm)	Crystallite size d(104) (nm)
VK	40.1%	77.9%	42.5	41.6	25.6	16.5
XL-VK-1	21.1%	70.4%	35.2	31.9	24.0	23.2
XL-VK-2	19.3%	66.9%	33.6	28.6	22.9	17.0
XL-VK-3	10.8%	62.8%	30.0	18.2	13.4	7.0

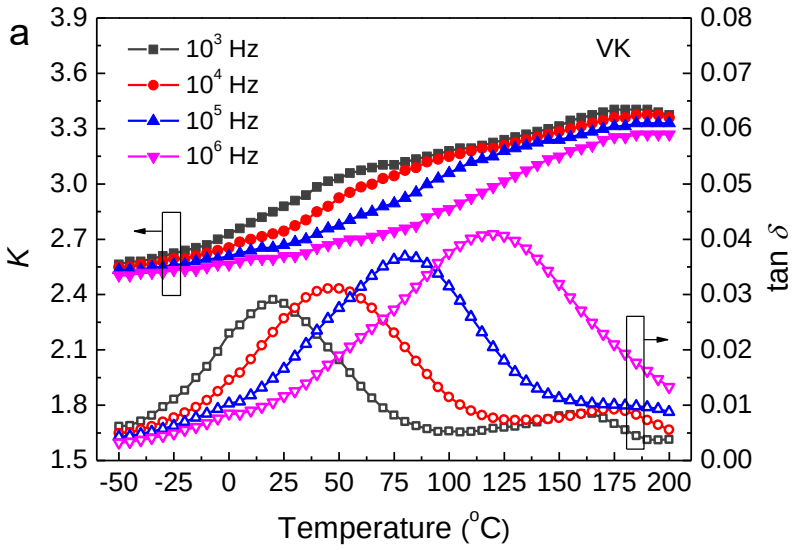
a
VK
10^3 Hz
10^4 Hz
10^5 Hz
10^6 Hz
K
tan δ
Temperature (°C)

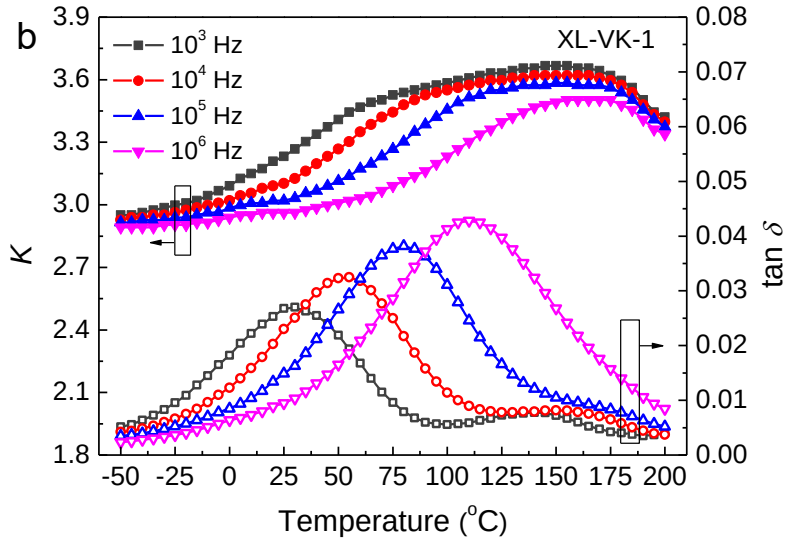
b
XL-VK-1
10^3 Hz
10^4 Hz
10^5 Hz
10^6 Hz
K
tan δ
Temperature (°C)

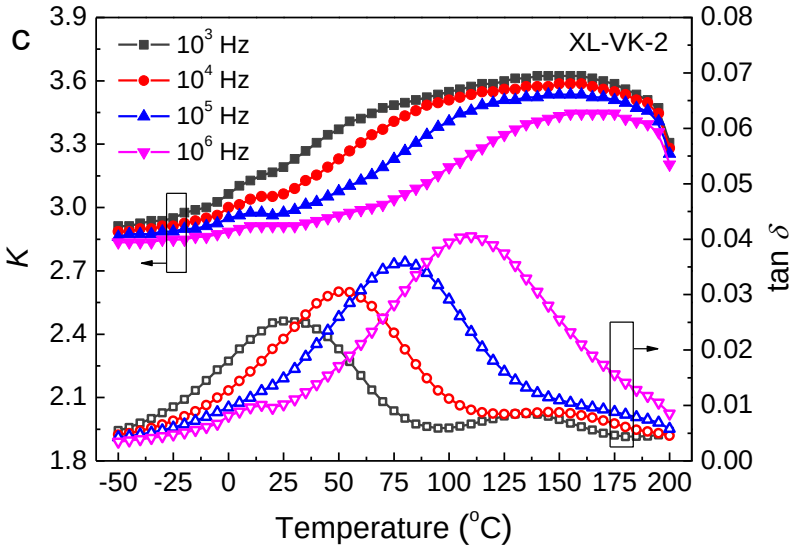
c
XL-VK-2
10^3 Hz
10^4 Hz
10^5 Hz
10^6 Hz
K
tan δ
Temperature (°C)

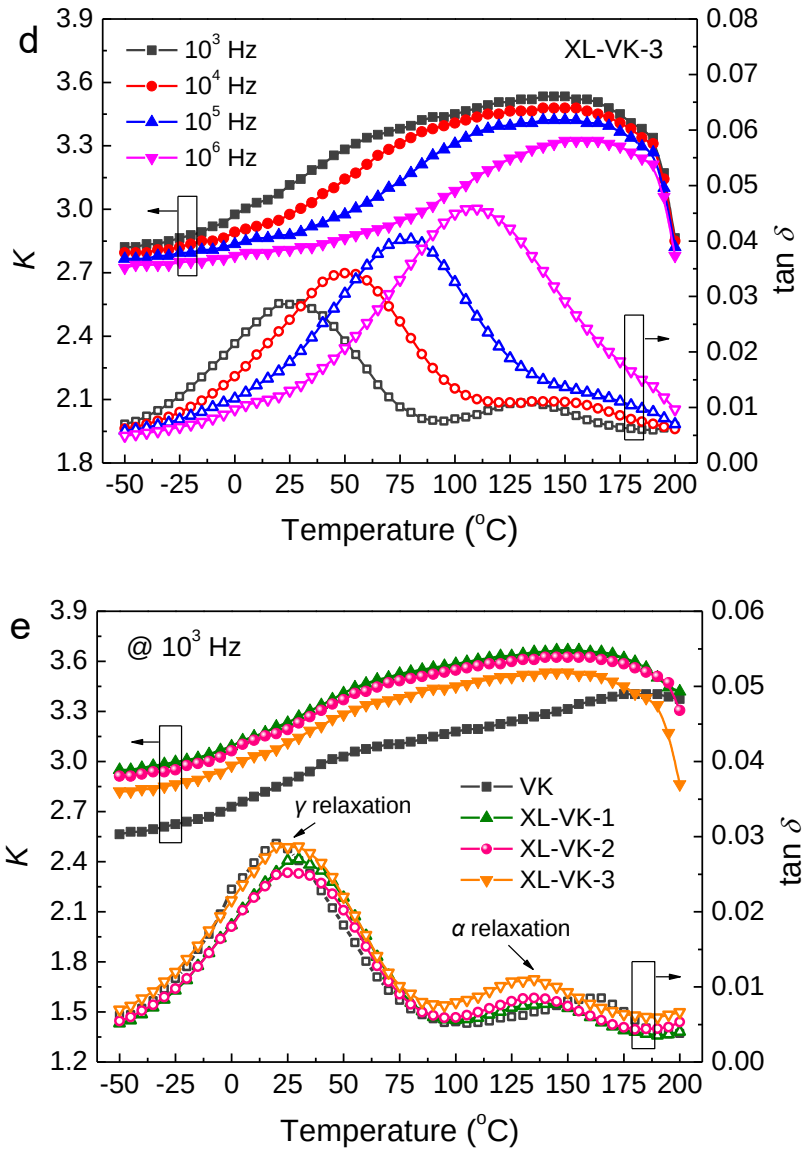

Fig. S9. Temperature-dependent dielectric spectra of the real part of permittivity (*K*) and loss tangent (tan δ) of (a) **VK**, (b) **XL-VK-1**, (c) **XL-VK-2**, (d) **XL-VK-3** at varied frequencies and (e) **VK** and **XL-VK** at 10^3 Hz.

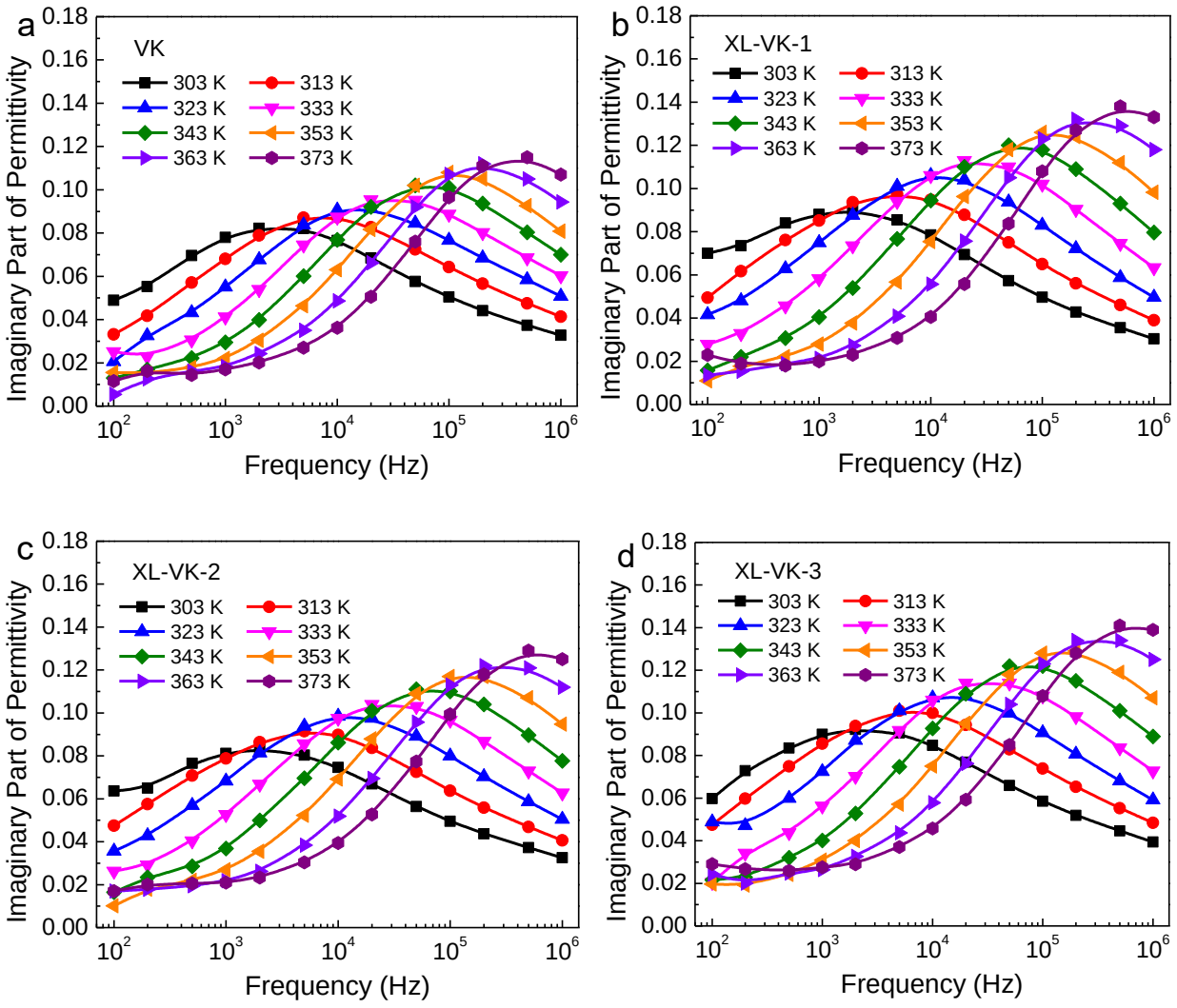

Fig. S10. Frequency-dependent dielectric spectra of the imaginary part of permittivity of (a) **VK**, (b) **XL-VK-1**, (c) **XL-VK-2**, (d) **XL-VK-3** at varied temperatures.

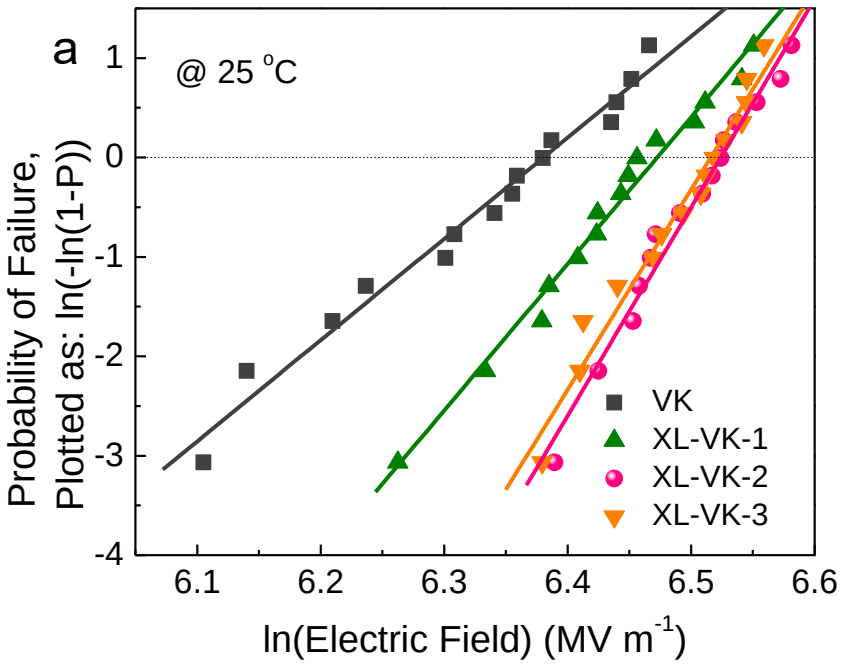
a
@ 25 °C
Probability of Failure,
Plotted as: ln(-ln(1-P))
1
0
-1
-2
-3
-4
6.1
6.2
6.3
6.4
6.5
6.6
ln(Electric Field) (MV m-1)
VK
XL-VK-1
XL-VK-2
XL-VK-3

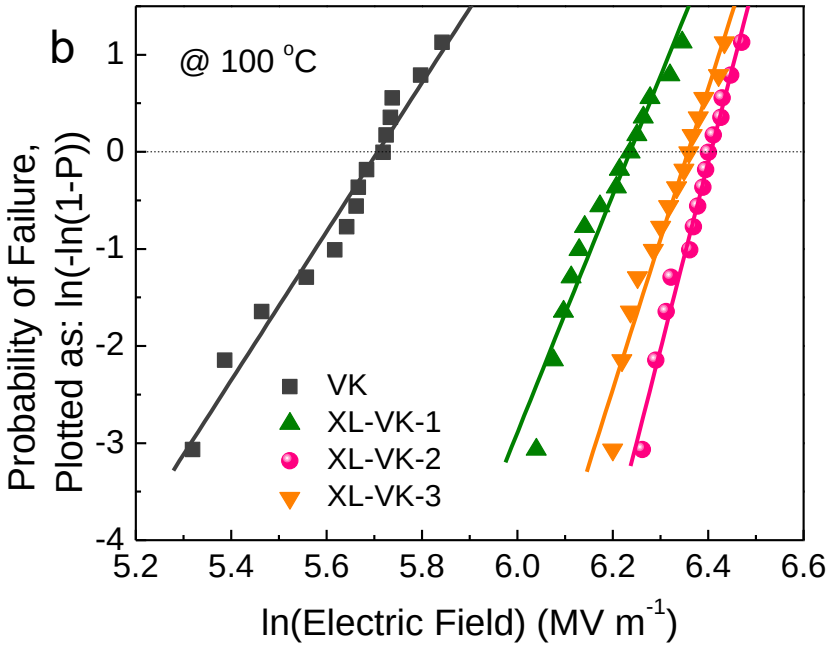
b
@ 100 °C
Probability of Failure,
Plotted as: ln(-ln(1-P))
1
0
-1
-2
-3
-4
5.2
5.4
5.6
5.8
6.0
6.2
6.4
6.6
ln(Electric Field) (MV m-1)
VK
XL-VK-1
XL-VK-2
XL-VK-3

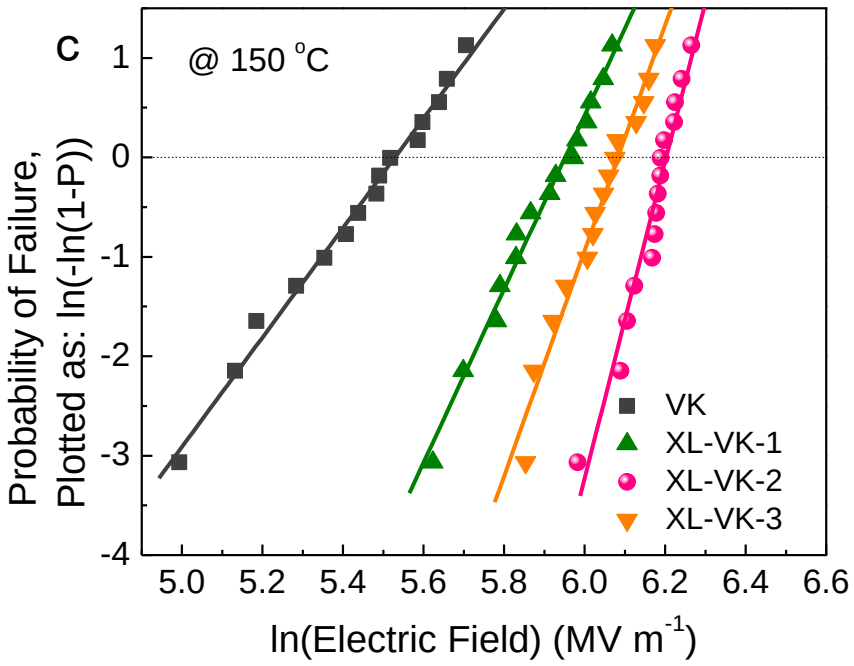

Fig. S11. Weibull statistic of dielectric breakdown strength of **VK** and **XL-VK** at (a) 25 °C, (b) 100 °C and (c) 150 °C.

Table S2. Weibull parameters of **VK** and **XL-VK** at varied temperatures.

Sample	25 °C		100 °C		150 °C	
	E_b (MV m^{-1})	β	E_b (MV m^{-1})	β	E_b (MV m^{-1})	β
VK	590	10.19	301	7.66	251	5.51
XL-VK-1	646	14.76	511	12.24	384	8.73
XL-VK-2	681	20.95	604	19.23	494	15.94
XL-VK-3	674	20.14	577	15.51	438	11.34

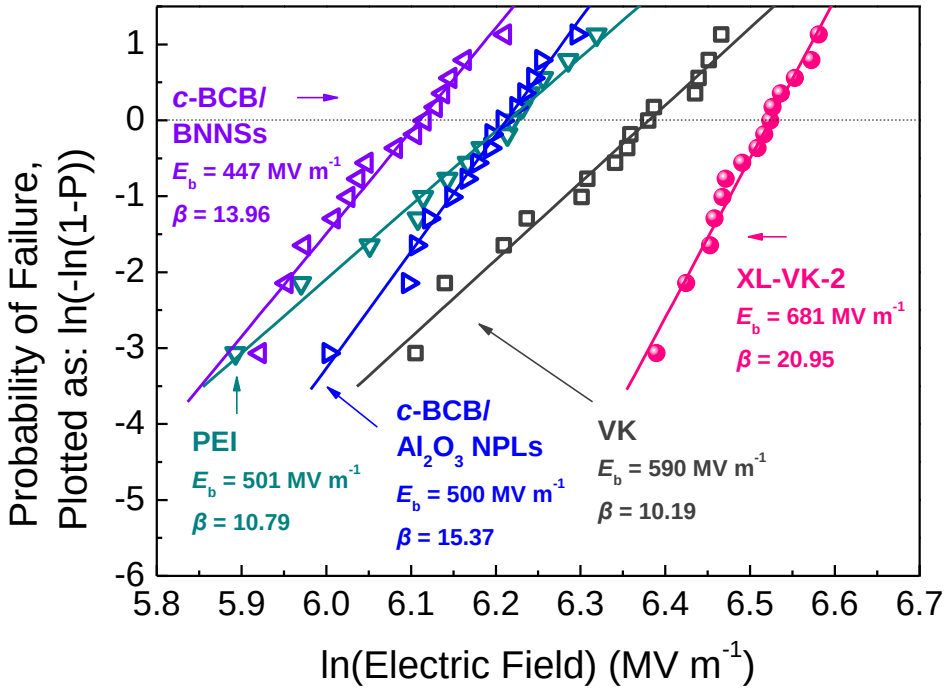

Fig. S12. Room-temperature Weibull breakdown strengths of **VK**, **XL-VK-2** and high-temperature dielectric polymer and composite dielectrics including PEI, *c*-BCB/BNNSs and *c*-BCB/Al_2O_3 NPLs.

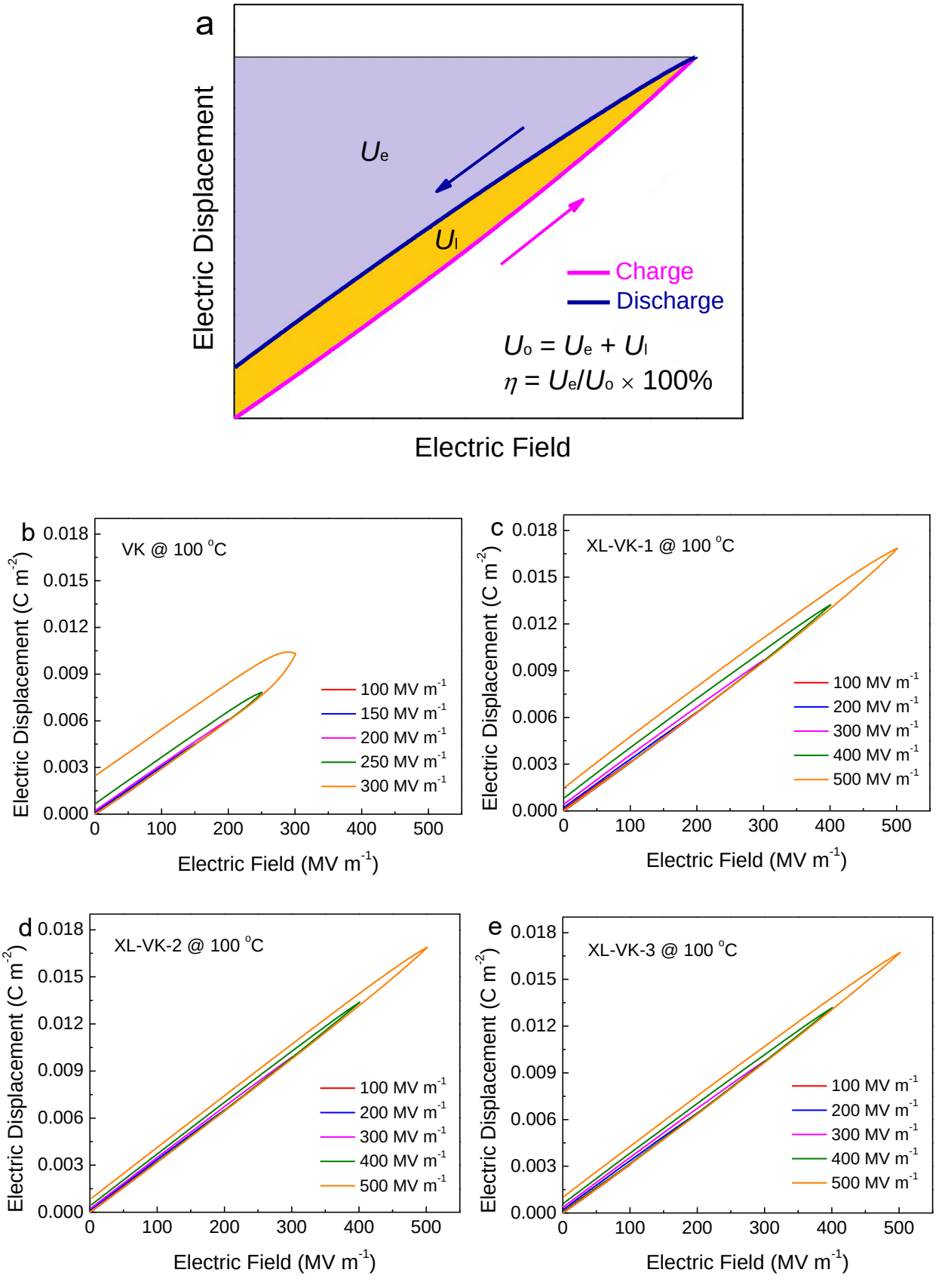
a
Electric Displacement
U_e
U_l
Charge
Discharge
$U_o = U_e + U_l$
$\eta = U_e/U_o \times 100\%$
Electric Field
b
VK @ 100 °C
Electric Displacement (C m^{-2})
0.000
0.003
0.006
0.009
0.012
0.015
0.018
0
100
200
300
400
500
Electric Field (MV m^{-1})
100 MV m^{-1}
150 MV m^{-1}
200 MV m^{-1}
250 MV m^{-1}
300 MV m^{-1}
c
XL-VK-1 @ 100 °C
Electric Displacement (C m^{-2})
Electric Field (MV m^{-1})
100 MV m^{-1}
200 MV m^{-1}
300 MV m^{-1}
400 MV m^{-1}
500 MV m^{-1}
d
XL-VK-2 @ 100 °C
Electric Displacement (C m^{-2})
Electric Field (MV m^{-1})
100 MV m^{-1}
200 MV m^{-1}
300 MV m^{-1}
400 MV m^{-1}
500 MV m^{-1}
e
XL-VK-3 @ 100 °C
Electric Displacement (C m^{-2})
Electric Field (MV m^{-1})
100 MV m^{-1}
200 MV m^{-1}
300 MV m^{-1}
400 MV m^{-1}
500 MV m^{-1}

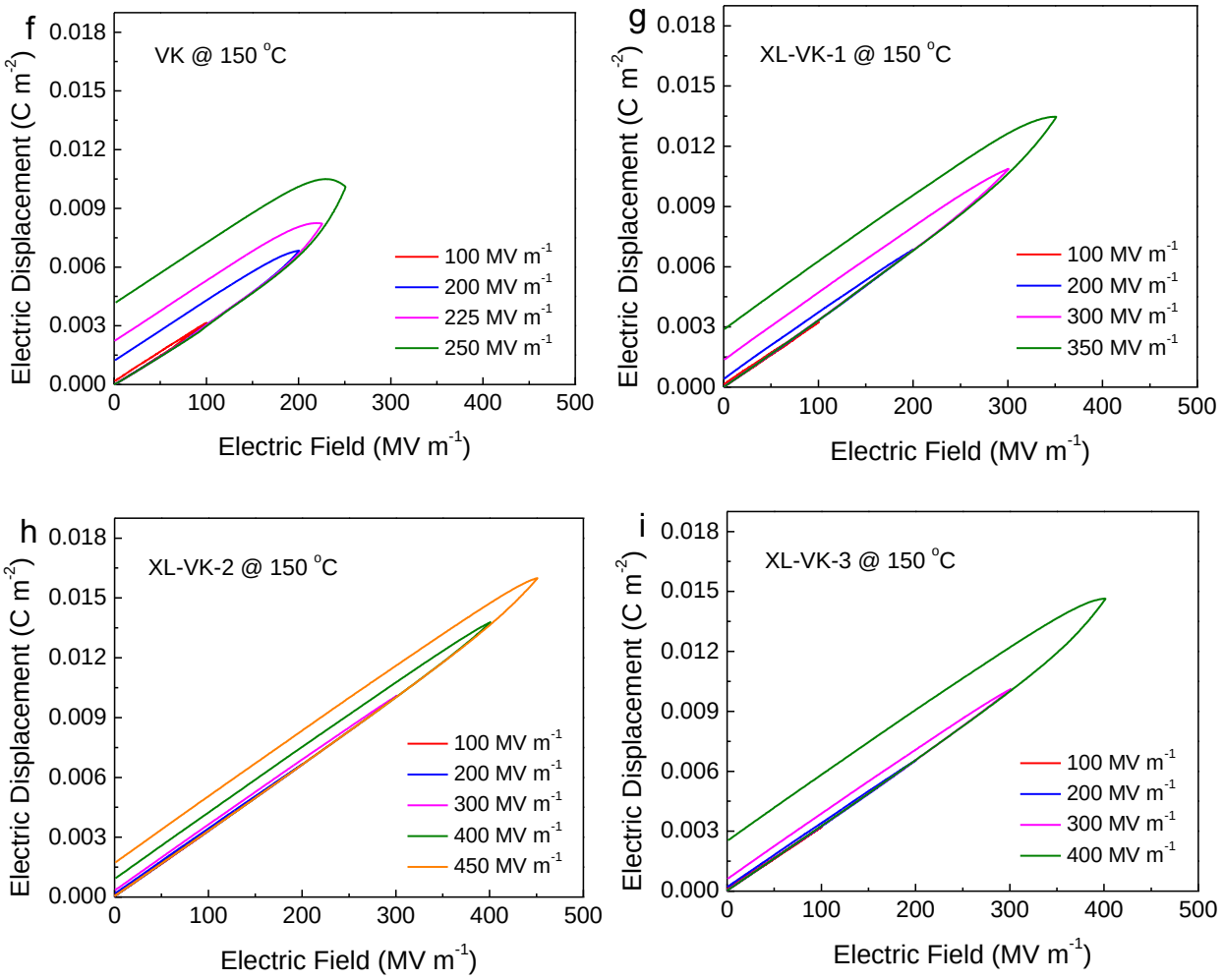

Fig. S13. (a) Schematic of electric displacement–electric field (*D*–*E*) loop of a dielectric material with the discharged energy density (U_e) represented by the area in painted purple and energy density loss (U_l) indicated by the area colored orange. The total stored energy density (U_o) equals U_e plus U_l, and the charge–discharge efficiency (η) is calculated by $\eta = U_e/U_o \times 100\%$. The conduction loss can be calculated as $U_l/U_o \times 100\%$. Unipolar *D*–*E* loops of **VK**, **XL-VK-1**, **-2**, and **-3** measured at 100 °C (b-e) and 150 °C (f-i), respectively.

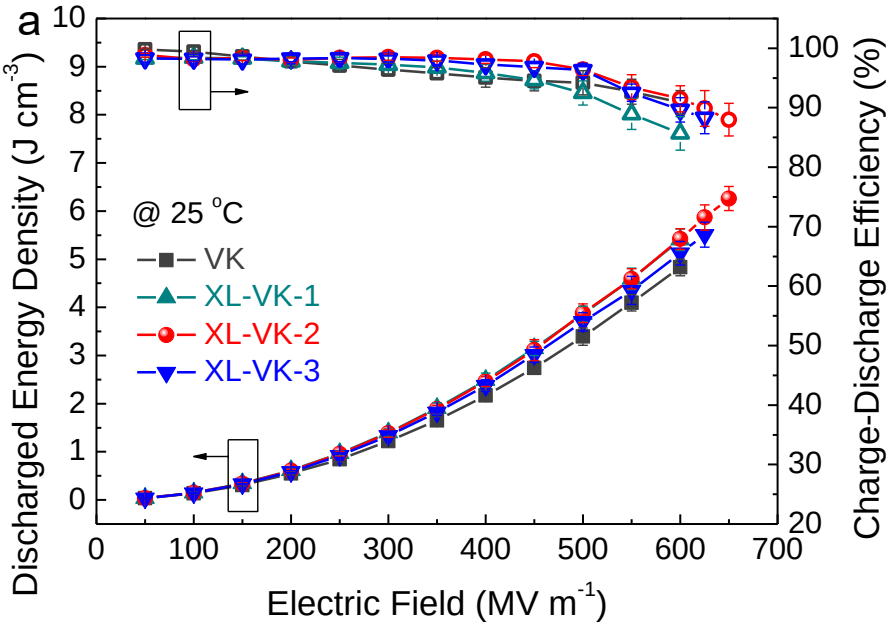
a
Discharged Energy Density (J cm-3)
Charge-Discharge Efficiency (%)
Electric Field (MV m-1)
@ 25 °C
VK
XL-VK-1
XL-VK-2
XL-VK-3

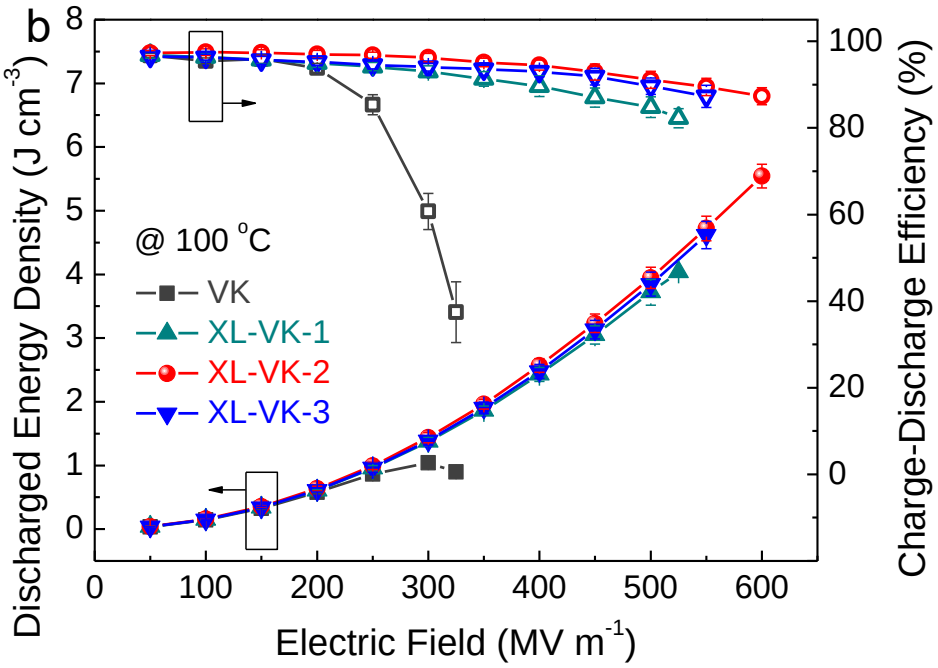
b
Discharged Energy Density (J cm-3)
Charge-Discharge Efficiency (%)
Electric Field (MV m-1)
@ 100 °C
VK
XL-VK-1
XL-VK-2
XL-VK-3

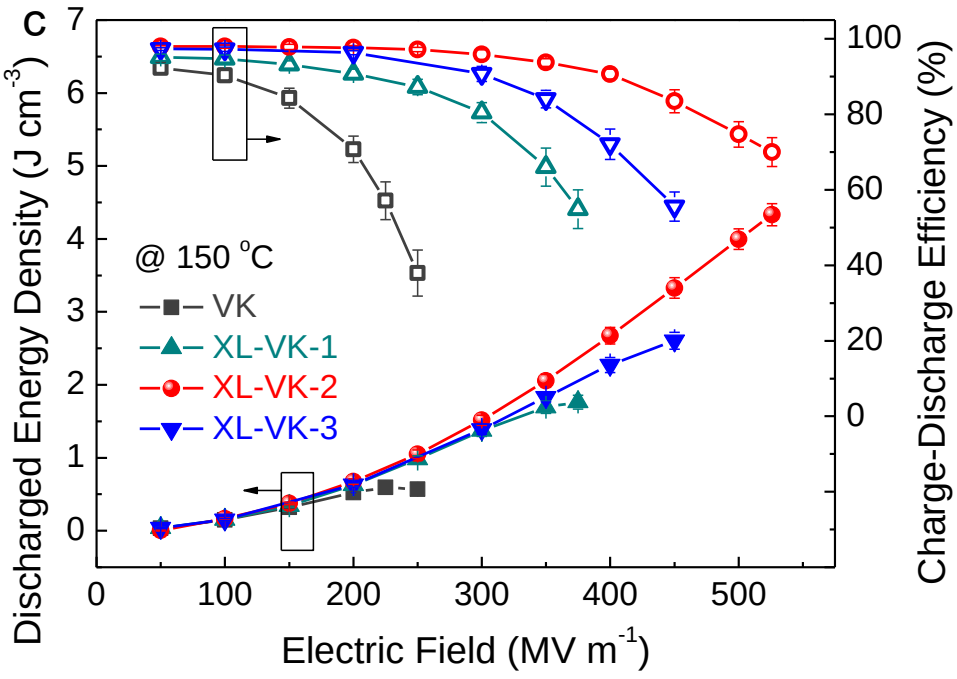

Fig. S14. Discharged energy density and charge–discharge efficiency of **VK** and **XL-VK** at (a) 25 °C, (b) 100 °C and (c) 150 °C. Error bars represent standard deviations obtained from at least three measurements using different samples.

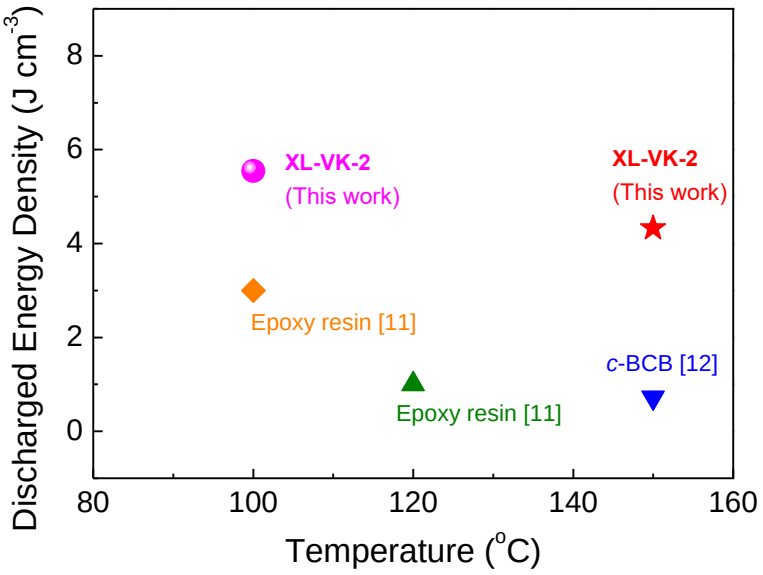

Fig. S15. Discharged energy density of **XL-VK-2** and other crosslinked polymer dielectrics at elevated temperatures.

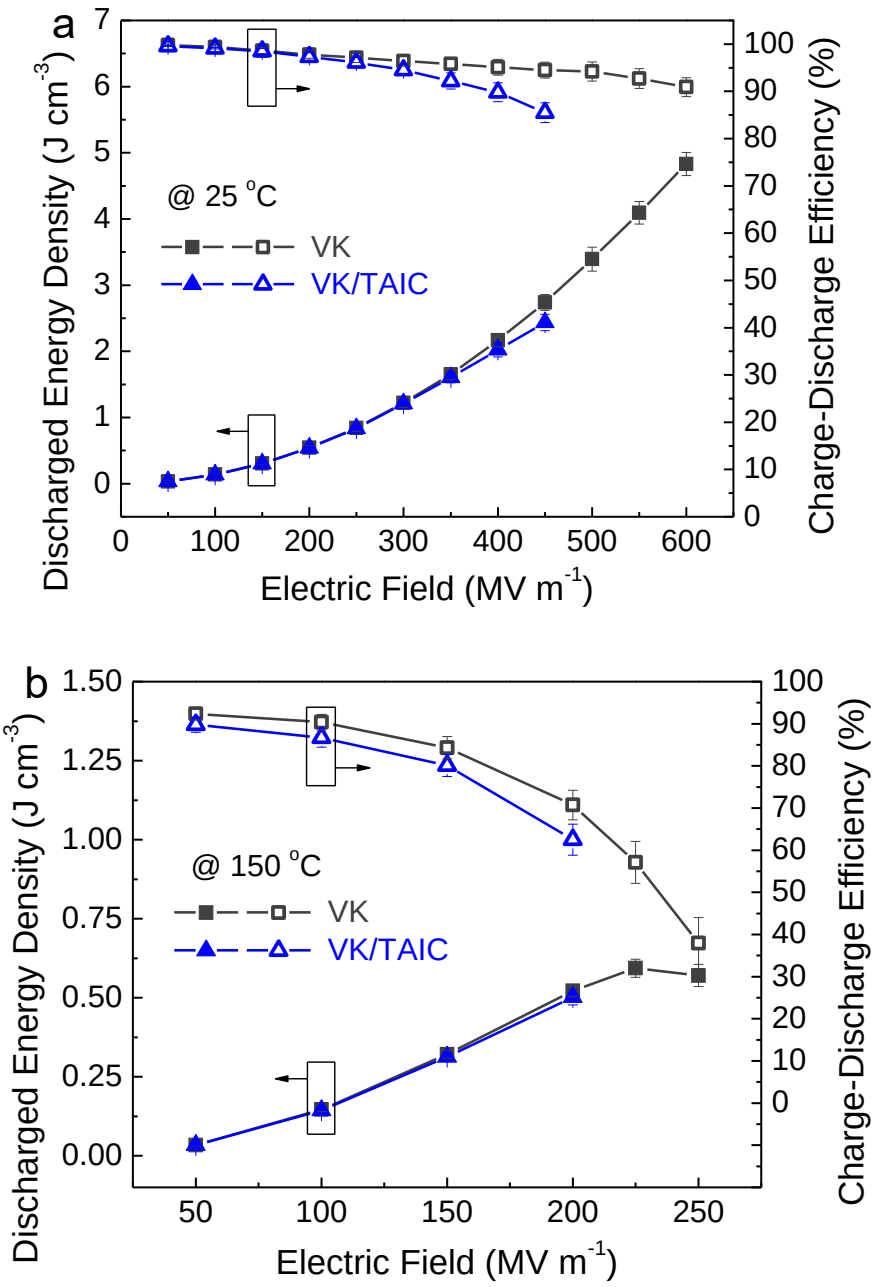

Fig. S16. Discharged energy density and charge–discharge efficiency of VK containing 5 wt% TAIC measured at (a) 25 °C and (b) 150 °C. Error bars represent standard deviations obtained from at least three measurements using different samples.

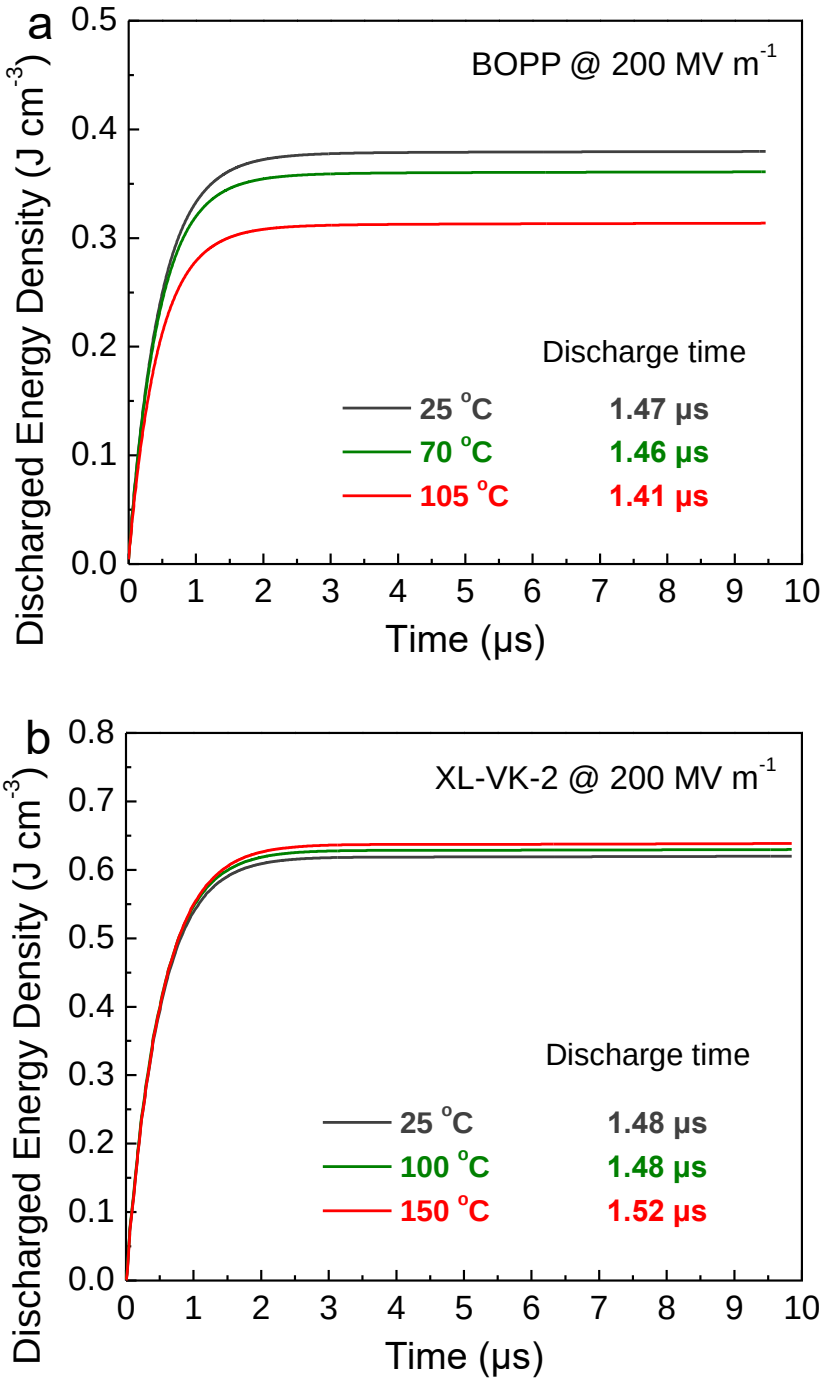

Fig. S17. Discharged energy density of (a) BOPP and (b) **XL-VK-2** at varied temperatures measured at 200 MV m^{-1} as a function of discharge time.

The discharge time ($t_{95\%}$) is defined as the time for the discharge energy in a load resistor to reach 95% of the final value. Power density (P) is given as

$$P = \frac{U_{95\%}}{t_{95\%}} \tag{S2}$$

where $U_{95\%}$ is the discharged energy density recorded at the discharge time.

In a typical fast discharge test, the stored energy was discharged to a resistor R_L in series with the sample[13]. Since the various losses in a dielectric material should also be treated as an equivalent series resistor (ESR), the energy discharged to R_L (U_R) is smaller than the total stored energy (U_o) in the sample, as interpreted by the equation given as

$$U_R = \frac{U_o * R_L}{R_L + \mathrm{ESR}} \tag{S3}$$

But when the R_L is much larger than the ESR, the discharged energy is very close to the stored one. And also, ESR will depend on the discharge speed (or R_L). In the frequency domain analysis,

$$\mathrm{ESR}(\omega) = \frac{\tan\delta}{\omega C} \tag{S4}$$

where ω is the angular frequency, and C is the capacitance. At the initial time of discharging (high frequencies) to R_L in which most of the energy is released, ESR effect is small. At later stage (longer time and lower frequencies) of discharging process, ESR influence increases.

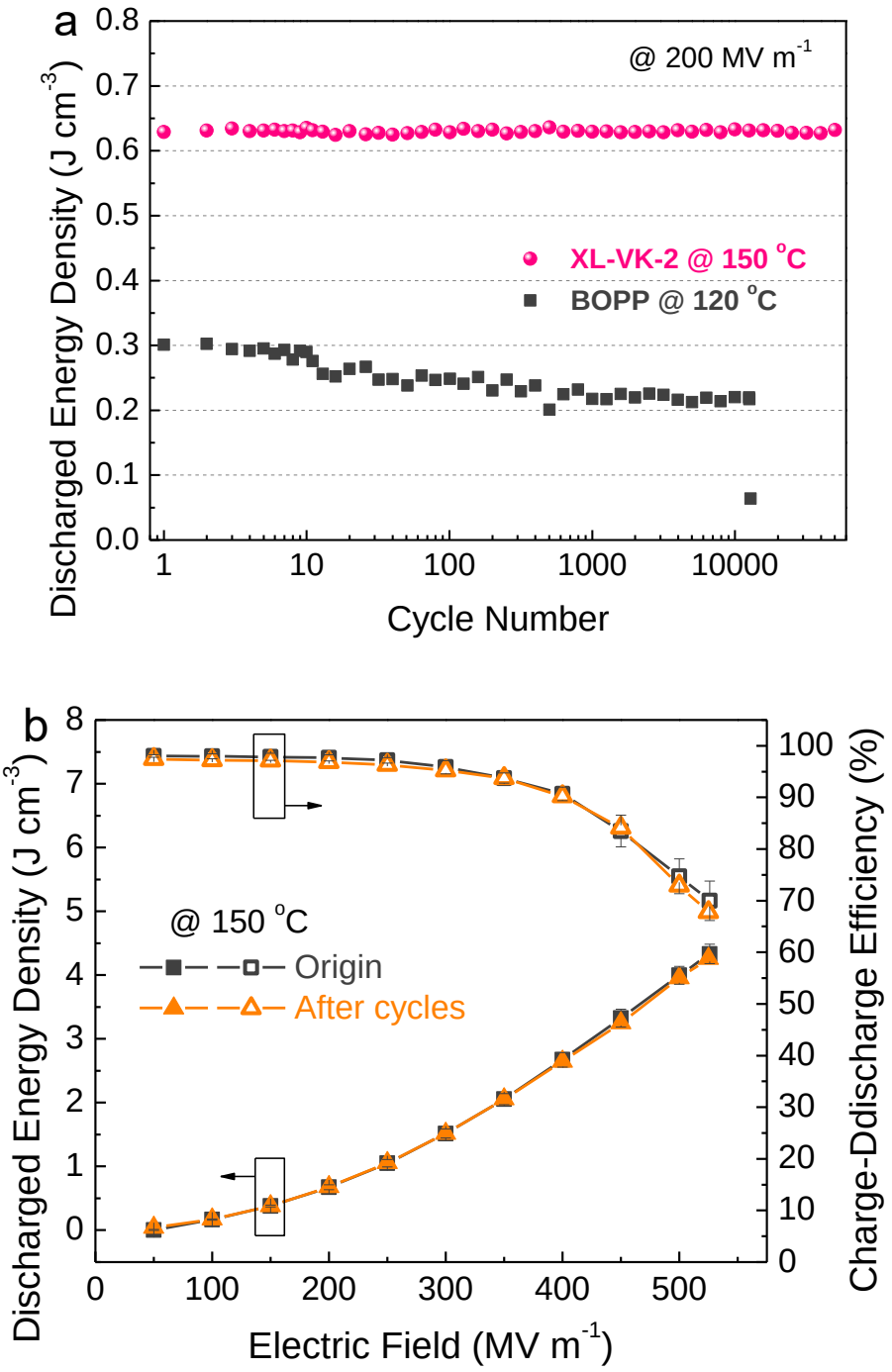

Fig. S18. (a) Cyclic ability of BOPP at 120 °C and **XL-VK-2** at 150 °C measured at 200 MV m^{-1}. **XL-VK-2** shows almost no sign of degradation in U_e over a straight 50,000 cycles at 150 °C, while BOPP is broken down at the 12,852 cycle at 120 °C.[14] (b) Capacitive performance of **XL-VK-2** before and after 50,000 cycling at 150 °C and 200 MV m^{-1}.

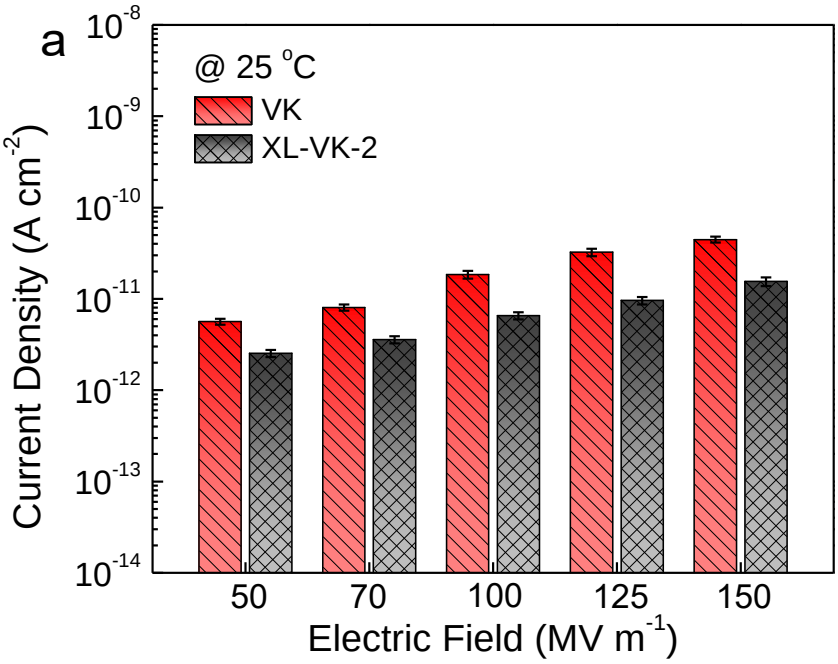
a
@ 25 °C
VK
XL-VK-2
Current Density (A cm-2)
10-8
10-9
10-10
10-11
10-12
10-13
10-14
50
70
100
125
150
Electric Field (MV m-1)

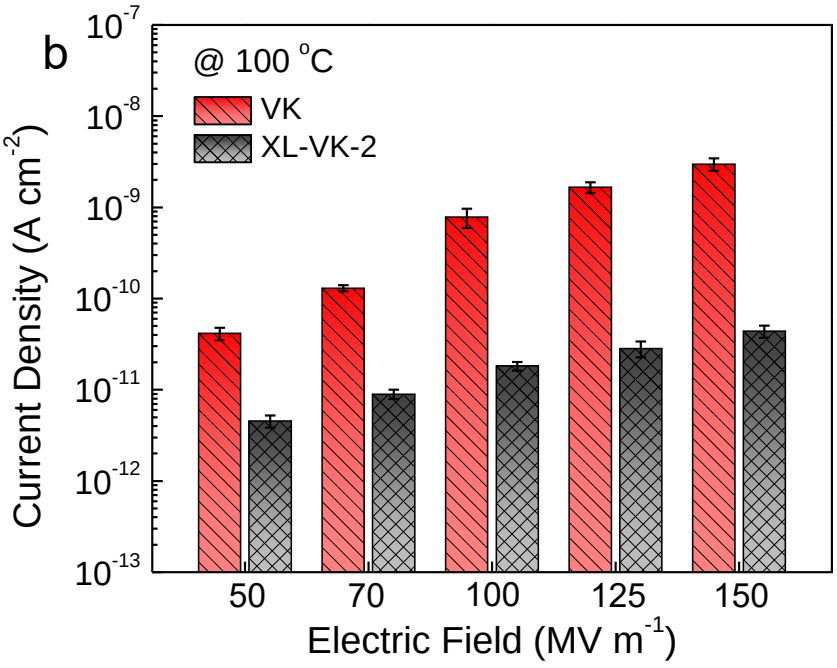
b
@ 100 °C
VK
XL-VK-2
Current Density (A cm-2)
10-7
10-8
10-9
10-10
10-11
10-12
10-13
50
70
100
125
150
Electric Field (MV m-1)

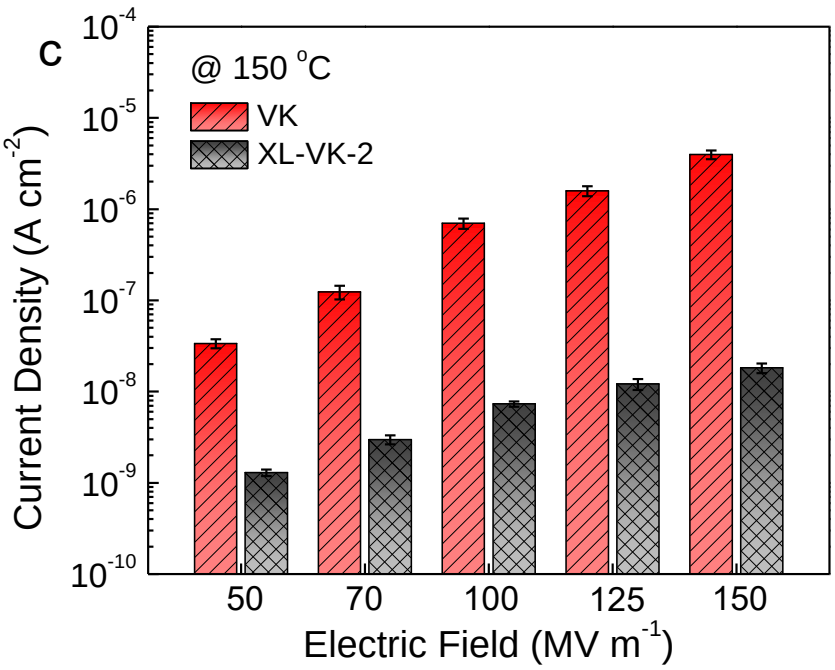

Fig. S19. Comparison of the conduction current density of **VK** and **XL-VK-2** measured at varied electric fields at (a) 25 ºC, (b) 100 ºC and (c) 150 ºC. Error bars represent standard deviations obtained from at least three measurements using different samples.

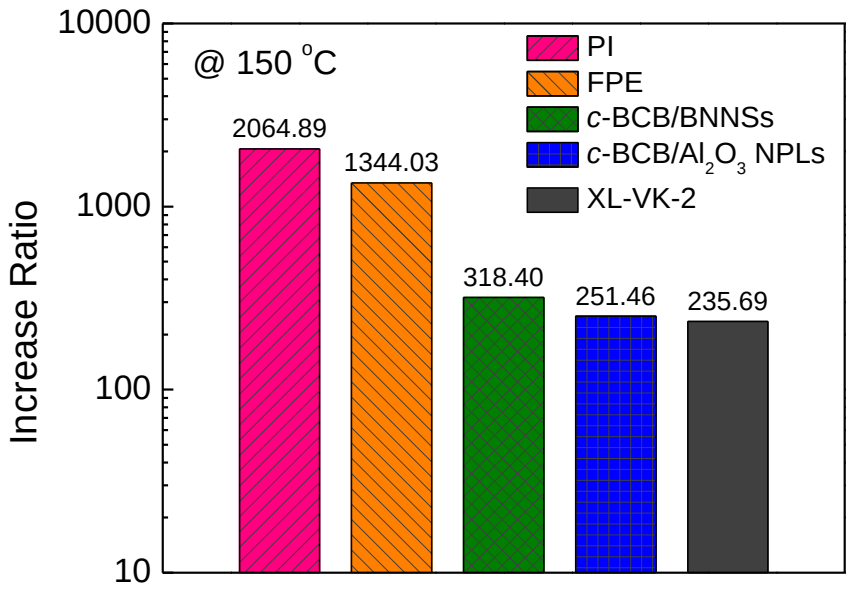

Fig. S20. Increase ratio of conduction current density of **XL-VK-2** and high-temperature dielectrics with the applied field at 400 MV m^{-1} *vs.* at 50 MV m^{-1} measured at 150 °C. The increase ratio of conduction current density (R_i) was calculated by

$$R_i = \frac{J_h}{J_l} \tag{S5}$$

where J_h is the conduction current density measured at relatively high electric field (*i.e.*, 400 MV m^{-1}) and J_l is the conduction current density measured at relatively low electric field (*i.e.*, 50 MV m^{-1}).

Table S3. TSDC results and calculated trap parameters

Sample	Peak current ($\times 10^{-12}$ A)	Peak temperature (T_m) (K)	Trap energy level (eV)	Trapped charge quantity (nC)
VK	1.11	144.50	0.57	0.86
XL-VK-1	5.90	158.30	0.89	5.76
XL-VK-2	15.27	160.20	1.03	13.12
XL-VK-3	20.66	154.50	0.96	17.64

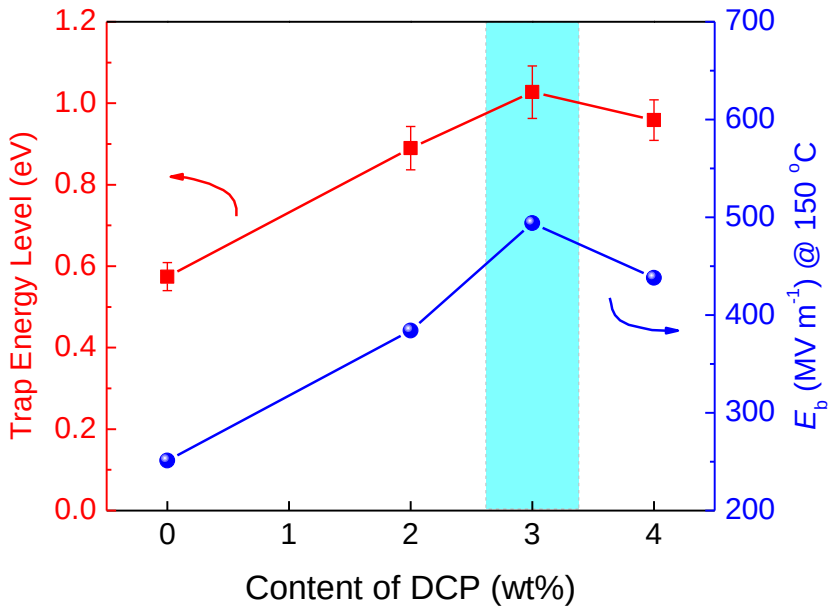

Fig. S21. Weibull Breakdown Strength (E_b) at 150 °C and trap energy level calculated from TSDC curve of **VK** and **XL-VK** as a function of DCP content. Error bars represent standard deviations obtained from at least three measurements using different samples. The formation of deepest traps and its high-temperature peak location at ~160 °C for **XL-VK-2** could be responsible for the improved dielectric breakdown strength up to 150 °C since[15,16]

$$E_b \propto \exp\left(\frac{A_{TSDC}}{4K_B T}\right) \quad \text{(S6)}$$

where A_{TSDC} is the trap energy level, K_B is the Boltzmann constant. Charges need to overcome a potential barrier after being trapped, the bigger the trap energy becomes, the stronger the trapping effect is. It is difficult for the trapped carriers in deeper traps to escape (de-trap), thus leading to the decreased carrier mobility and the improvement of breakdown strength.

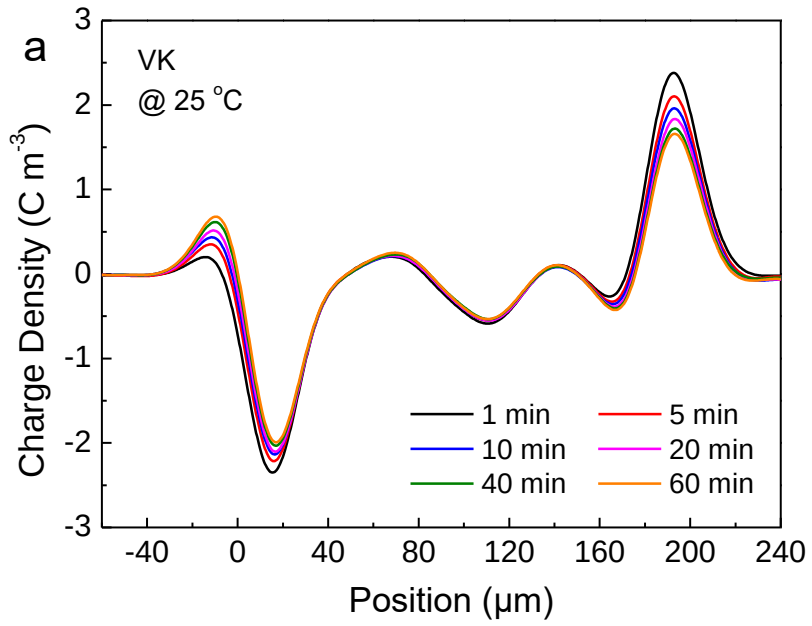
a
VK
@ 25 °C
Charge Density (C m-3)
Position (μm)
1 min
5 min
10 min
20 min
40 min
60 min

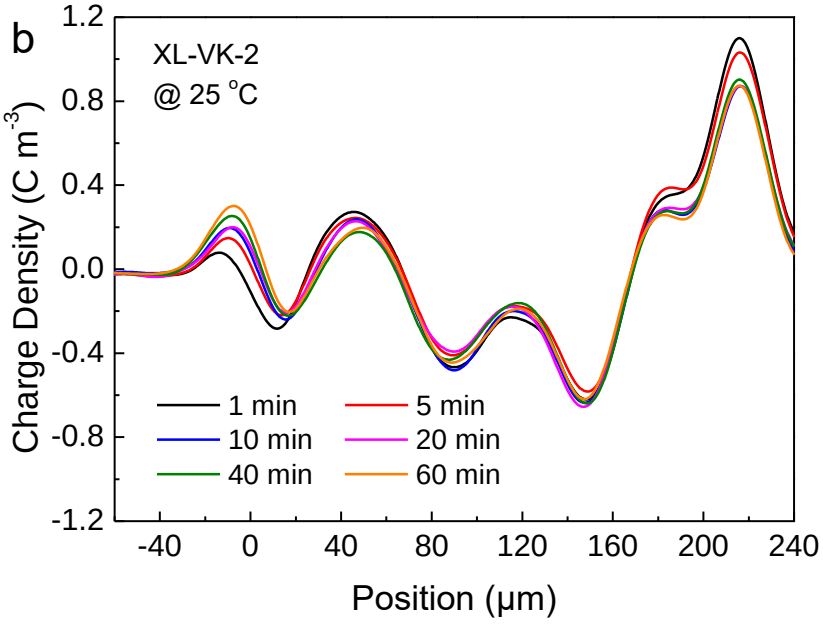
b
XL-VK-2
@ 25 °C
Charge Density (C m-3)
Position (μm)
1 min
5 min
10 min
20 min
40 min
60 min

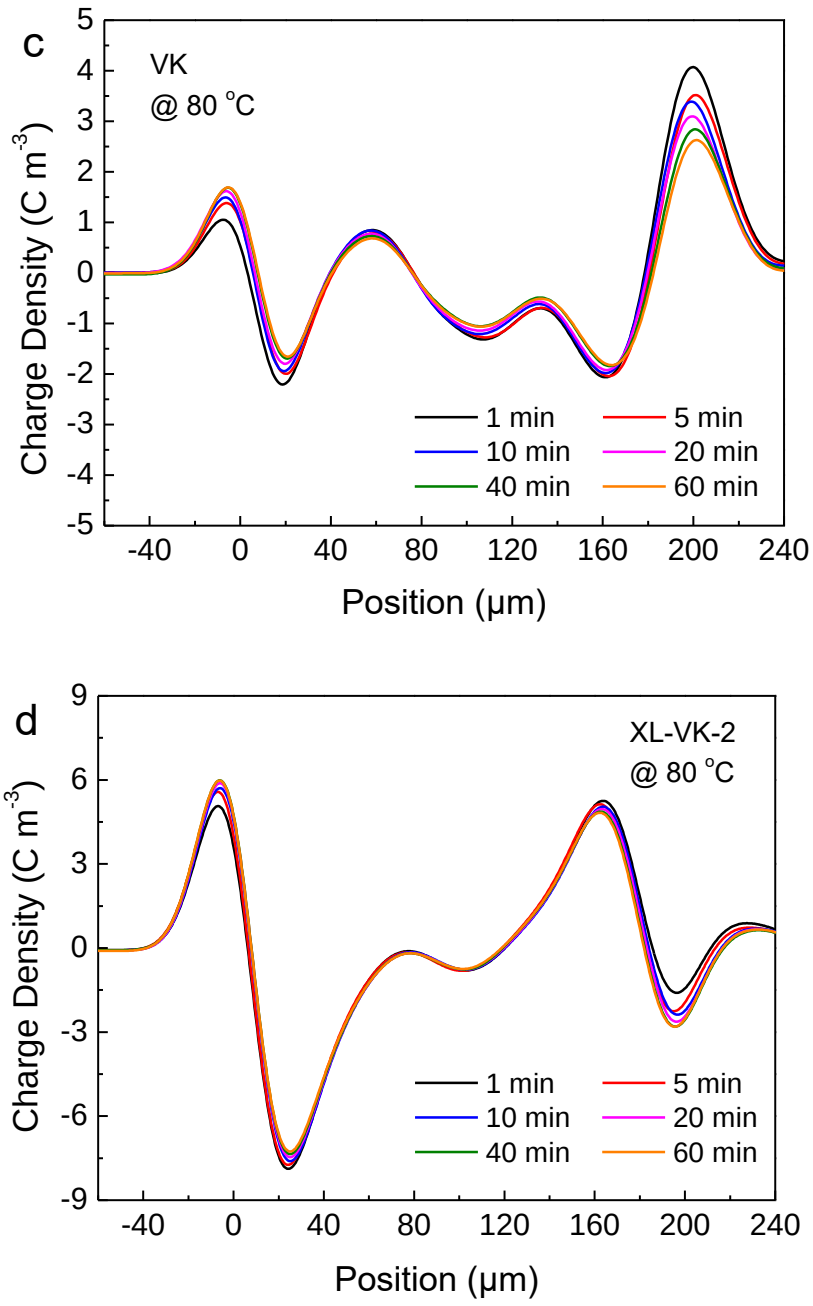

Fig. S22. Charge decay profiles of **VK** and **XL-VK-2** at 25 ºC (a,b) and 80 ℃ (c,d), respectively.

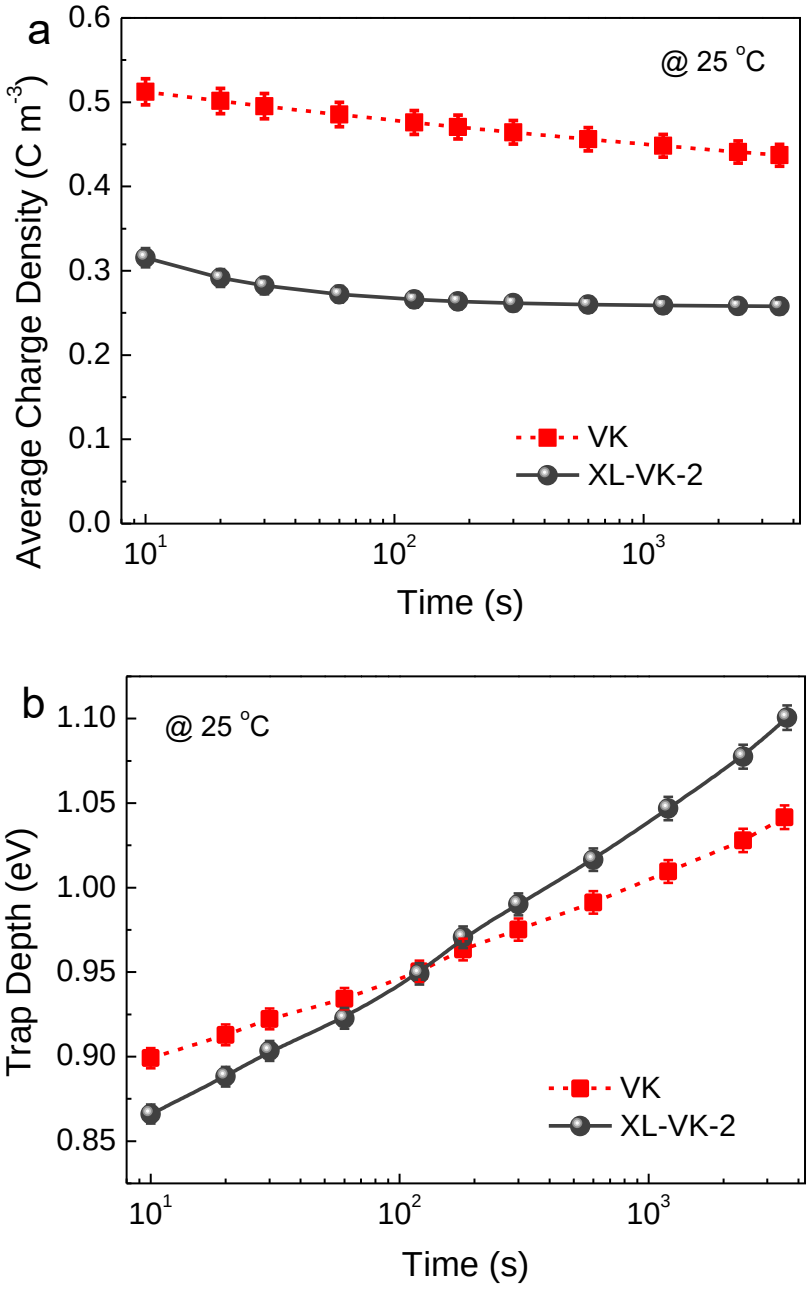
a
@ 25 °C
Average Charge Density (C m-3)
0.6
0.5
0.4
0.3
0.2
0.1
0.0
VK
XL-VK-2
10^1
10^2
10^3
Time (s)
b
@ 25 °C
Trap Depth (eV)
1.10
1.05
1.00
0.95
0.90
0.85
VK
XL-VK-2
10^1
10^2
10^3
Time (s)

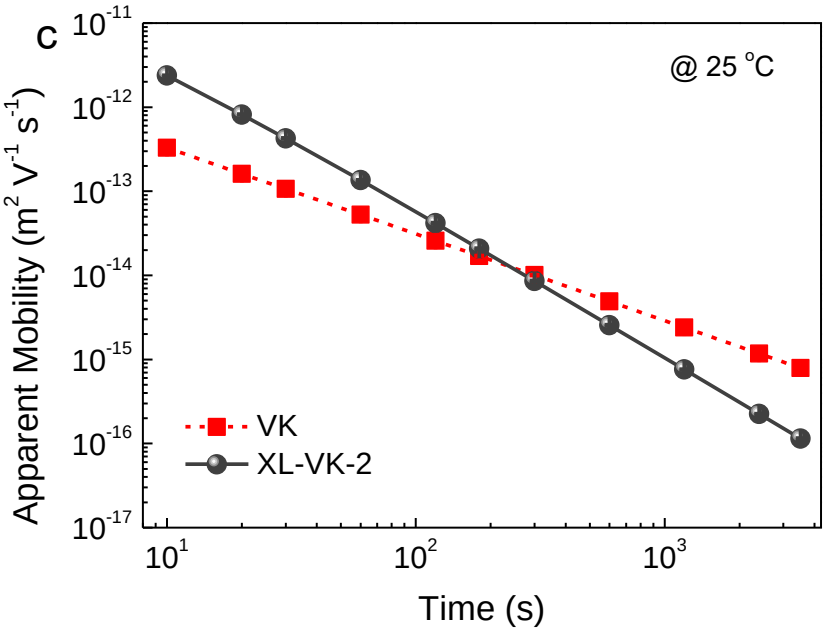

Fig. S23. (a) Average charge density, (b) Trap depth, and (c) Apparent mobility of **VK** and **XL-VK-2** as a function of decay time at 25 ºC, respectively. Error bars represent standard deviations obtained from at least three measurements using different samples.

Supplementary References

1. A. Taguet, B. Ameduri and B. Boutevin, *Adv. Polym. Sci*., Springer Press, New York, 2005, 127.
2. D. J. T. Hill, K. J. Thurecht and A. K. Whittaker, *Radiat. Phys. Chem.*, 2003, **67**, 729.
3. Y. Suzuoki, K. Yasuda, T. Mizutani and M. Ieda, *J. Phys. D Appl. Phys.*, 1977, **10**, 1985.
4. Y. Takai, K. Mori, T. Mizutani and M. Ieda, *Jpn. J. Appl. Phys.*, 1976, **15**, 2341.
5. C. Y. Liang and S. Krimm, *J. Chem. Phys.*, 1956, **25**, 563.
6. A. Soldera, *Macromolecular Symposia*, WILEY-VCH Verlag GmbH & Co. KGaA, Weinheim, 1998, 11.
7. A. M. Bueche, *J. Am. Chem. Soc.*, 1952, **74**, 65.
8. N. S. Murthy, Y. P. Khanna and A. J. Signorelli, *Polym. Eng. Sci.*, 1994, **34**, 1254.
9. P. Starck, *Polym. Int.*, 1996, **40**, 111.
10. P. Khanchaitit, K. Han, M. R. Gadinski, Q. Li and Q. Wang, *Nat. Commun.*, 2013, **4**, 2845.
11. S. Chen, G. Meng, B. Kong, B. Xiao, Z. Wang, Z. Jing, Y. Gao, G. Wu, H. Wang and Y. Cheng, *Chem. Eng. J.*, 2020, **387**, 123662.
12. Q. Li, L. Chen, M. R. Gadinski, S. Zhang, G. Zhang, H. U. Li, E. Iagodkine, A. Haque, L. Q. Chen, T. Jackson and Q. Wang, *Nature*, 2015, **523**, 576.
13. Q. Li, K. Han, M. R. Gadinski, G. Zhang and Q. Wang, *Adv. Mater.*, 2014, **26**, 6244.
14. H. Li, L. Ren, D. Ai, Z. Han, Y. Liu, B. Yao and Q. Wang, *InfoMat*, 2020. DOI: 10.1002/inf2.12043.
15. S. J. Wang, J. W. Zha, W. K. Li and Z. M. Dang, *Appl. Phys. Lett.*, 2016, **108**, 092902.
16. S. Li, D. Xie, G. Qu, L. Yang, D. Min and Y. Cheng, *Appl. Surf. Sci.*, 2019, **478**, 451.